Anomalous superconductivity and its competition with antiferromagnetism in doped Mott insulators

S. S. Kancharla,[1] B. Kyung,[1] D. Sénéchal,[1] M. Civelli,[2,3] M. Capone,[4] G. Kotliar,[2] and A.-M. S. Tremblay[1]

[1]*Département de Physique and Regroupement Québécois sur les Matériaux de Pointe, Université de Sherbrooke, Sherbrooke, Québec, Canada J1K 2R1*

[2]*Department of Physics and Center for Materials Theory, Rutgers University, Piscataway, New Jersey 08854, USA*

[3]*Theory Group, Insiitut Laue Langevin, Grenoble, France*

[4]*SMC, CNR-INFM, and Physics Department, University of Roma "La Sapienza," Piazzale A. Moro 2, I-00185 Rome, Italy and ISC-CNR, Via dei Taurini 19, I-00185 Rome, Italy*

Proximity to a Mott insulating phase is likely to be an important physical ingredient of a theory that aims to describe high-temperature superconductivity in the cuprates. Quantum cluster methods are well suited to describe the Mott phase. Hence, as a step toward a quantitative theory of the competition between antiferromagnetism and d-wave superconductivity in the cuprates, we use cellular dynamical mean-field theory to compute zero-temperature properties of the two-dimensional square lattice Hubbard model. The d-wave order parameter is found to scale like the superexchange coupling J for on-site interaction U comparable to or larger than the bandwidth. The order parameter also assumes a dome shape as a function of doping, while, by contrast, the gap in the single-particle density of states decreases monotonically with increasing doping. In the presence of a finite second neighbor hopping t', the zero-temperature phase diagram displays the electron-hole asymmetric competition between antiferromagnetism and superconductivity that is observed experimentally in the cuprates. Adding realistic third neighbor hopping t'' improves the overall agreement with the experimental phase diagram. Since band parameters can vary depending on the specific cuprate considered, the sensitivity of the theoretical phase diagram to band parameters challenges the commonly held assumption that the doping vs T_c/T_c^{max} phase diagram of the cuprates is universal. The calculated angle-resolved photoemission spectrum displays the observed electron-hole asymmetry. The tendency to homogeneous coexistence of the superconducting and antiferromagnetic order parameters is stronger than observed in most experiments but consistent with many theoretical results and with experiments in some layered high-temperature superconductors. Clearly, our calculations reproduce important features of d-wave superconductivity in the cuprates that would otherwise be considered anomalous from the point of view of the standard Bardeen–Cooper–Schrieffer approach. At strong coupling, d-wave superconductivity and antiferromagnetism naturally appear as two equally important competing instabilities of the normal phase of the same underlying Hamiltonian.

PACS number(s): 71.10.Fd, 71.35.−y, 72.80.Sk, 78.30.Am

I. INTRODUCTION

Superconductivity in the cuprates and in the layered organics of the BEDT family is highly anomalous, i.e., it displays a number of properties that cannot be explained by the Bardeen–Cooper–Schrieffer (BCS) theory modified for d-wave symmetry. For example, in the cuprates, superconductivity emerges upon doping an antiferromagnetic Mott insulator. Moreover, in the so-called underdoped region near the insulator, experiments show that the gap in the single-particle density of states decreases upon doping while T_c/T_c^{max} or the order parameter increases, which is in sharp contrast with expectations from standard BCS theory.[1] In the organics, antiferromagnetism and superconductivity are separated by a first-order transition and a Mott transition separates the corresponding states with no order. For both the organics and the cuprates, there is much evidence from approximate solutions that the essential low-energy physics is described by the one-band Hubbard model for the appropriate lattice, band structure, interaction, and dopings.[2–4]

Theoretically understanding anomalous superconductivity in a quantitative manner is still a challenge. An important step toward this goal is to obtain accurate solutions of the Hubbard model. Despite the apparent simplicity of the model, it is extremely difficult to solve in the relevant regime where neither the potential (U) nor the kinetic energy ($8t$) dominate. In recent years, a number of numerical methods have shed light on this problem. In this paper, we will describe the results obtained from the cellular dynamical mean-field theory[5] (CDMFT) for d-wave superconductivity and its competition with antiferromagnetism in the cuprates. The corresponding study in the organics has been published.[6,7] The results will be compared with other quantum cluster methods,[8–10] mean-field theories, slave boson, and with variational approaches.

Our choice of method is motivated by the following considerations. Since anomalous superconductivity appears near antiferromagnetic Mott insulating phases, it is important to use approaches that correctly treat these phases. CDMFT is a generalization of the dynamical mean-field theory (DMFT).[11,12] The latter method describes the Mott insulator-metal transition of the Hubbard model exactly in the limit of infinite dimensions. DMFT is, by construction, a local theory that maps the full interacting many-body lattice problem onto a single-site embedded in a self-consistent bath. Unfortunately, the local nature of the spatial correlations inherent

to single-site DMFT precludes a description of the superconducting phase with d-wave symmetry experimentally observed in the cuprates. This limitation has been overcome by several recently developed cluster extensions of DMFT. In addition to CDMFT,[5] these include the dynamical cluster approximation (DCA)[13] and variational cluster perturbation theory,[14,15] which is also known as the variational cluster approximation (VCA). These methods incorporate short-range correlations as well as some properties of the infinite lattice in a systematic and causal manner (for reviews, see Refs. 8–10). CDMFT maps a lattice problem onto a finite-size cluster (with different boundary conditions than DCA) and is able to accurately describe the short-range correlations within the cluster. A self-consistently determined bath of uncorrelated electrons approximates the effect of the rest of the infinite lattice on the cluster. Coupling between the embedded cluster and the bath provides a self-consistent theory that naturally allows for phase transitions and phases with long-range order. In a way, CDMFT makes a compromise between short-range and long-range correlations, the latter being associated with order parameters that appear only in the bath.

Cluster models can be formulated in a general functional framework[10,15] and they all converge to the same limit for very large cluster sizes. Nevertheless, different cluster methods have convergence rates that depend on the physical observable. In particular, at finite temperatures, CDMFT has been shown to converge exponentially quickly for local quantities such as the density of states.[16] The quality of the approximation made by CDMFT has been tested extensively by comparisons with exact results.[17,18] The method was found to be accurate in describing the complexities of the Mott insulator-to-metal transition, indicating that both high and low energy phenomena are well captured. Furthermore, CDMFT has also been successfully used to elucidate the differences in the evolution of a Mott–Hubbard insulator into an anomalous correlated metal for the electron- and hole-doped cases[19,20] as well as to shed light on the normal state pseudogap phenomenon.[21]

In the following section, we describe our implementation of CDMFT in more detail. We then present the zero-temperature results and compare to those of other numerical approaches. It is shown that, in the intermediate-coupling regime $U=8t$, the d-wave superconducting phase at zero temperature is stabilized. In addition, at strong coupling, the magnitude of the order parameter scales with $J=4t^2/U$. We also discuss the effect of longer-range hopping and of the proximity to the Mott transition. We present the phase diagram for both hole- and electron-doped systems, exhibiting the competition between d-wave superconductivity and antiferromagnetism. The regions where d-wave superconductivity and antiferromagnetism appear are in semiquantitative agreement with experiment, except for a region of coexistence that is not always observed experimentally. It is striking to observe that as we make the model more realistic by including all the main band structure parameters t, t', and t'', the coexistence region decreases and the overall phase diagram becomes closer to experiments. Finally, before we summarize the results, we compute the single-particle density of states and show that the order parameter increases with doping in contrast to the single-particle gap that decreases, which is in qualitative agreement with experiment. In addition, we find that the results of angle-resolved photoemission spectroscopy (ARPES)[22] have a natural explanation in our approach. Discussion of our results in the context of a sample of the existing literature appears at the end of each subsection.

II. MODEL AND METHODS

We define the Hubbard model Hamiltonian by

$$H = -\sum_{i,j,\sigma} t_{i,j} d_{i,\sigma}^\dagger d_{j,\sigma} + U \sum_i n_{i\uparrow} n_{i\downarrow}, \qquad (1)$$

where $t_{i,j}$ and U correspond to the hopping and the on-site Coulomb repulsion, respectively. In order to investigate the d-wave superconducting phase within CDMFT, we write an effective action containing a Weiss dynamical field $\hat{\mathcal{G}}_0$ with both normal (particle-hole) and anomalous (particle-particle) components that describe the degrees of freedom outside the cluster (the bath) as a time dependent hopping within the cluster,

$$S_{\text{eff}} = \int_0^\beta d\tau d\tau' \Psi_d^\dagger(\tau) [\hat{\mathcal{G}}_0^{-1}] \Psi_d(\tau') + U \sum_\mu \int_0^\beta d\tau n_{\mu\uparrow} n_{\mu\downarrow}. \qquad (2)$$

For the case of a 2×2 plaquette, which we shall consider throughout this work, the Nambu spinor is defined by $\Psi_d^\dagger \equiv (d_{1\uparrow}^\dagger, \ldots, d_{4\uparrow}^\dagger, d_{1\downarrow}, \ldots, d_{4\downarrow})$ and μ, ν label the degrees of freedom within the cluster. Physically, this action corresponds to a cluster embedded in a self-consistently determined medium with d-wave pairing correlations.

Given the effective action with a starting guess for the Weiss field $\hat{\mathcal{G}}_0$, we compute the cluster propagator $\hat{G}_c$ by solving the cluster impurity Hamiltonian that will be shortly described. Then, we extract the cluster self-energy from $\hat{\Sigma}_c = \hat{\mathcal{G}}_0^{-1} - \hat{G}_c^{-1}$. Here,

$$\hat{G}_c(\tau, \tau') = \begin{pmatrix} \hat{G}_\uparrow(\tau, \tau') & \hat{F}(\tau, \tau') \\ \hat{F}^\dagger(\tau, \tau') & -\hat{G}_\downarrow(\tau', \tau) \end{pmatrix} \qquad (3)$$

is an 8×8 matrix, while $G_{\mu\nu,\sigma} \equiv -\langle T d_{\mu\sigma}(\tau) d_{\nu\sigma}^\dagger(0) \rangle$ and $F_{\mu\nu} \equiv -\langle T d_{\mu\uparrow}(\tau) d_{\nu\downarrow}(0) \rangle$ are the imaginary-time-ordered normal and anomalous Green functions, respectively. Using the self-consistency condition

$$\hat{\mathcal{G}}_0^{-1}(i\omega_n) = \left[\frac{N_c}{(2\pi)^2} \int d\tilde{\mathbf{k}} \hat{G}(\tilde{\mathbf{k}}, i\omega_n) \right]^{-1} + \hat{\Sigma}_c(i\omega_n), \qquad (4)$$

with

$$\hat{G}(\tilde{\mathbf{k}}, i\omega_n) = [i\omega_n + \mu - \hat{t}(\tilde{\mathbf{k}}) - \hat{\Sigma}_c(i\omega_n)]^{-1}, \qquad (5)$$

we recompute the Weiss field $\hat{\mathcal{G}}_0^{-1}$ and iterate will convergence. Here, $\hat{t}(\tilde{\mathbf{k}})$ is the Fourier transform of the superlattice hopping matrix with appropriate sign flip between propagators for up and down spins and the integral over $\tilde{\mathbf{k}}$ is per-

formed over the reduced Brillouin zone of the superlattice.

To solve the cluster impurity problem represented by the effective action above, we express it in the form of a Hamiltonian H_{imp} with a discrete number of bath orbitals coupled to the cluster and use the exact-diagonalization technique (Lanczos method),[23]

$$H_{imp} \equiv \sum_{\mu\nu\sigma} E_{\mu\nu\sigma} d^{\dagger}_{\mu\sigma} d_{\nu\sigma} + \sum_{m\sigma} \epsilon^{\alpha}_{m\sigma} a^{\dagger\alpha}_{m\sigma} a^{\alpha}_{m\sigma}$$
$$+ \sum_{m\mu\sigma} V^{\alpha}_{m\mu\sigma} a^{\dagger\alpha}_{m\sigma} (c_{\mu\sigma} + \mathrm{H.c.}) + U \sum_{\mu} n_{\mu\uparrow} n_{\mu\downarrow}$$
$$+ \sum_{\alpha} \Delta^{\alpha} (a^{\alpha}_{1\uparrow} a^{\alpha}_{2\downarrow} - a^{\alpha}_{2\uparrow} a^{\alpha}_{3\downarrow} + a^{\alpha}_{3\uparrow} a^{\alpha}_{4\downarrow} - a^{\alpha}_{4\uparrow} a^{\alpha}_{1\downarrow} + a^{\alpha}_{2\uparrow} a^{\alpha}_{1\downarrow}$$
$$- a^{\alpha}_{3\uparrow} a^{\alpha}_{2\downarrow} + a^{\alpha}_{4\uparrow} a^{\alpha}_{3\downarrow} - a^{\alpha}_{1\uparrow} a^{\alpha}_{4\downarrow} + \mathrm{H.c.}).$$

Here, $\mu, \nu = 1, \ldots, N_c$ label the sites in the cluster and $E_{\mu\nu\sigma}$ represents the hopping and the chemical potential within the cluster. The energy levels in the bath are grouped into replicas of the cluster ($N_c = 4$) (two replicas in the present case) with the labels $m = 1, \ldots, N_c$ and $\alpha = 1, 2$ such that we have 16 bath energy levels $\epsilon^{\alpha}_{m\sigma}$ coupled to the cluster via the bath-cluster hybridization matrix $V^{\alpha}_{m\mu\sigma}$. Using lattice symmetries, we take $V^{\alpha}_{m\mu\sigma} \equiv V^{\alpha} \delta_{m\mu}$ and $\epsilon^{\alpha}_{m\sigma} \equiv \epsilon^{\alpha}$. The quantity Δ^{α} represents the amplitude of superconducting correlations in the bath. No static mean-field order parameter directly acts on the cluster sites.[24]

The parameters ϵ^{α}, V^{α}, and Δ^{α} are determined by imposing the self-consistency condition in Eq. (4) using a conjugate gradient minimization algorithm with a distance function

$$d = \sum_{\omega_n, \mu, \nu} |[\hat{\mathcal{G}}'^{-1}_0(i\omega_n) - \hat{\mathcal{G}}^{-1}_0(i\omega_n)]_{\mu\nu}|^2 \qquad (6)$$

that emphasizes the lowest frequencies of the Weiss field by imposing a sharp cutoff at $\omega_c = 1.5$. (Energies are given in units of hopping t, and we take $\hbar = 1$ and $k_B = 1$.) The distance function in Eq. (6) is computed on the imaginary frequency axis (effective inverse temperature, $\beta = 50$) since the Weiss field $\hat{\mathcal{G}}_0(i\omega_n)$ is a smooth function on that axis.

With the bond superconducting order parameter defined as

$$\psi_{\mu\nu} = \langle d_{\mu\uparrow} d_{\nu\downarrow} \rangle, \qquad (7)$$

we consider a d-wave singlet pairing ($\psi \equiv \psi_{12} = -\psi_{23} = \psi_{34} = -\psi_{41}$). The average is taken in the ground state of the cluster.

To study the competition with antiferromagnetism, while preserving bipartite symmetry, hybridization $V^{\alpha}_{m\mu\sigma} \equiv V^{\alpha}_{\sigma} \delta_{m\mu}$ and bath site energies $\epsilon^{\alpha}_{m\sigma} \equiv \epsilon^{\alpha}_{\sigma}$ become spin dependent. This doubles the number of independent hybridization and bath parameters. The staggered magnetic order parameter is given by the cluster wave function average

$$M_{\mu} = \langle d^{\dagger}_{\mu\uparrow} d_{\mu\uparrow} - d^{\dagger}_{\mu\downarrow} d_{\mu\downarrow} \rangle, \qquad (8)$$

with $M \equiv M_1 = -M_2 = M_3 = -M_4$.

The finite size of the bath in the exact-diagonalization technique is an additional approximation to the CDMFT scheme. The accuracy of this approximation can be verified by comparing the CDMFT solution for the one-band Hubbard model with the solution from the Bethe ansatz.[18,25] We have also used this comparison in one dimension as a guideline to fix the choice of parameters in the distance function ($\omega_c = 1.5$ and $\beta = 50$). These results in one dimension also compare well with those obtained using the Hirsch–Fye quantum Monte Carlo algorithm as an impurity solver where the bath is not truncated.[26] Further, using finite-size scaling for these low (but finite) temperature calculations,[26] it was shown that, at intermediate to strong coupling, a 2×2 cluster in a bath accounts for more than 95% of the correlation effect of the infinite-size cluster in the single-particle spectrum.

We can also perform an internal consistency check on the effect of the finite bath on the accuracy of the calculation. With an infinite bath, convergence ensures that the density inside the cluster is identical to the density computed from the lattice Green function. In practice, we find that there can be a difference of ±0.02 between the density estimated from the lattice and that estimated from the cluster. We will display results as a function of cluster density since benchmarks with the one-dimensional Hubbard model show that, with a finite bath and the procedure described above, one can quite accurately reproduce Bethe ansatz results for $n(\mu)$ when the cluster density is used. Nevertheless, we should adopt a conservative attitude and keep in mind the error estimate mentioned above.

III. ANOMALOUS SUPERCONDUCTIVITY AND ITS COMPETITION WITH MAGNETISM

In this section, we first discuss d-wave superconductivity by itself. Competition with magnetism is taken into account in subsequent subsections. We will conclude with single-particle spectral properties.

A. Scaling as J at strong coupling

The effect of interaction strength on d-wave superconductivity is illustrated in Fig. 1(a), where we show the d-wave order parameter ψ as a function of the density n for $t' = 0$ and different values of on-site Coulomb repulsion U. No long-range antiferromagnetism is allowed in this calculation. As U is increased to $8t$, the order parameter acquires a very broad maximum around $\delta = |1 - n| = 0.15$ (optimal doping). The d-wave Weiss field (not shown), on the other hand, is monotonic as a function of doping with a maximum value close to half-filling. As the system approaches half-filling from optimal doping, there is a progressive localization due to the increasing proximity of the Mott insulator and hence, despite the stronger d-wave Weiss field in this region, there is a suppression of the d-wave order parameter. This suppression is not seen for $U = 4t$ that is too small for a Mott transition. However, even in that case, if we were to allow for long-range antiferromagnetic correlations, the insulating gap at half-filling that emerges from antiferromagnetic (Slater) correlations should also d-wave superconductivity completely suppress.[27,28] Clearly, antiferromagnetism near half-filling can destroy superconductivity but the paramagnetic Mott transition by itself, without antiferromagnetism, suffices at strong to intermediate coupling. The maximum of the order
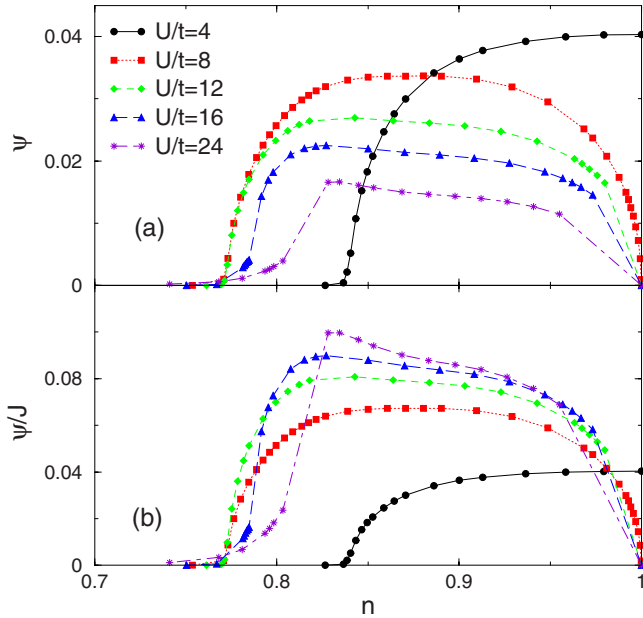
FIG. 1. (Color online) (a) *d*-wave order parameter ψ as a function of filling *n* and on-site Coulomb repulsion *U*, $t'=0$. (b) Same results but with the vertical axis divided by $J=4t^2/U$.

parameter increases as *U* increases but then it decreases as *U* changes to 12*t*, 16*t*, and 24*t*. This clearly signals that *d*-wave superconductivity will be strongest at intermediate coupling and that at strong coupling the *d*-wave order parameter scales as the superexchange coupling $J=4t^2/U$. In Fig. 1(b), the value of the order parameter is divided by *J* on the vertical axis to better exhibit this scaling for $U \geq 12t$. The value of optimal doping is nearly independent of *U* in the intermediate to strong coupling regime.

In the overdoped side, *d*-wave superconductivity disappears at a doping that is comparable to the DCA[13,29] and VCA.[30] Variational calculations[31,32] find *d*-wave superconductivity up to about 35% doping. The strong-coupling scaling with the superexchange coupling $J=4t^2/U$ as well as the domelike shape of the superconducting order parameter, which are a hallmark of correlated superconductivity, were also found in VCA,[30] renormalized mean-field theory,[33] gauge theories,[34] and in early RVB slave-boson studies.[35,36] In multiorbital models for fullerenes, a dome behavior is also found as a function of the correlation strength.[37,38] We note that at large doping for $U=8t-12t$, we find in Fig. 1 that the fall of the *d*-wave order parameter occurs with a constant negative curvature as a function of doping, which seems to occur experimentally. This contrasts with weak-coupling studies[27,28] where this does not occur.

Recent experiments[39] in four families (different *x*) of high-temperature superconductors $(Ca_xLa_{1-x})(Ba_{1.75-x}La_{0.25+x})Cu_3O_y$ suggest that scaling with *J* has been observed experimentally in the cuprates.

B. Effect of second neighbor hopping t'/t without competition with antiferromagnetism

The effect of next-nearest-neighbor hopping t'/t is illustrated in Fig. 2, where we plot the *d*-wave order parameter ψ
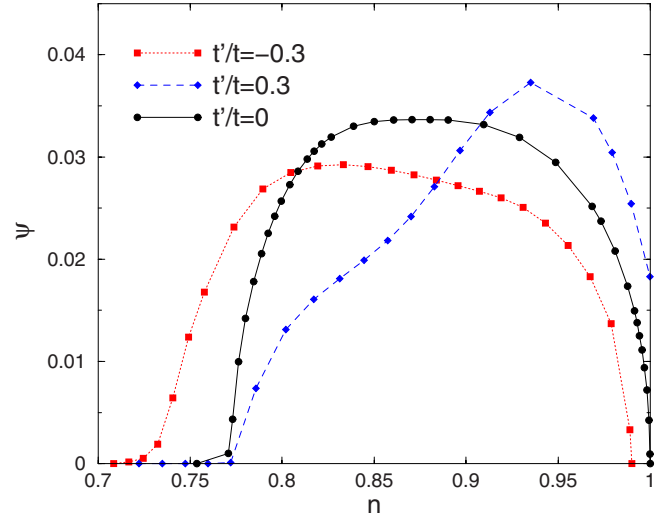

FIG. 2. (Color online) *d*-wave order parameter for $U=8t$ as a function of filling *n* for various values of t'/t (frustration).

as a function of doping for various values of the next-nearest-neighbor (diagonal) hopping t'. For clarity, we represent both the hole- and electron-doped cases on the same plot by performing a particle-hole transformation and considering $t'=+0.3t$ in the electron-doped case. The maximum of ψ grows with increasing t'.

This trend with t' was found in DCA,[29] in recent variational studies,[40] and in two-leg ladder studies of the $t-t'-J$ model.[41] However, the increase of ψ with t' does not seem consistent with the empirical correlation found in Ref. 42 between a larger optimal T_c and a smaller value of the t' obtained from band structure calculations. As found in an earlier VCA study,[30] the maximum ψ is larger for electron doping than for hole doping when calculations are done on 2×2 clusters. However, the situation reverses for larger clusters. This suggests that finite-size effects may be influencing our conclusions on the effect of t'. Superconductivity is known to be strongest on the hole-doped compounds as opposed to the electron-doped compounds (Using particle-hole transformation, the latter correspond to positive t' in Fig. 2). Nevertheless, we will see in the following section that including the competition with antiferromagnetism restores the experimentally observed electron-hole asymmetry.

C. Phase diagram and competition with magnetism

In the previous sections, we have constrained the bath of the associated impurity problem to allow only normal state and *d*-wave superconducting solutions. In this section, we start from initial bath parameters that allow for both *d*-wave and antiferromagnetic symmetry breaking. Figure 3 displays the results for the zero-temperature phase diagram for $t'=-0.3t$ and three values of the interaction strength $U=6t$, $U=8t$, and $U=12t$. The plots are as a function of electron density, so that the system is hole doped for $n<1$ and electron-doped for $n>1$. The order parameter for *d*-wave superconductivity is multiplied by a factor of 10 so that it is on the same scale as the antiferromagnetic order parameter. We
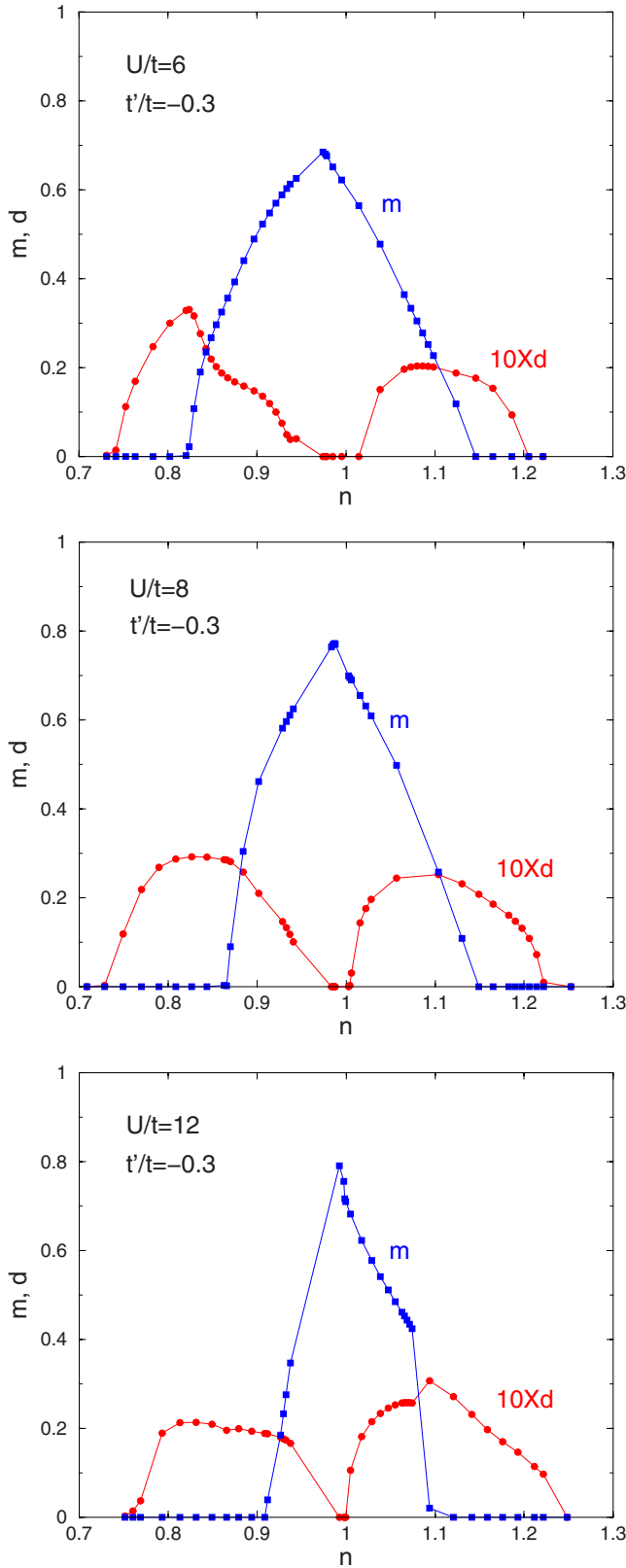
FIG. 3. (Color online) Superconducting (red circles) and antiferromagnetic (blue squares) order parameters for $t' = -0.3t$ and, from top to bottom, the three values $U = 6t$, $U = 8t$, and $U = 12t$. The amplitude of the superconducting order parameter is multiplied by a factor of 10 to be on a scale comparable to the antiferromagnetic one.

have checked that in the coexistence region, even if we start the iterations with a fully converged antiferromagnetic solution, the final solution is the same as the one exhibited in Fig. 3.

From Fig. 3, we observe that antiferromagnetism occurs over a narrower range of dopings as U increases since J then decreases (the trend would be opposite at weak coupling). There is a homogeneous coexistence of antiferromagnetism and d-wave superconductivity near half-filling in all cases. That phase can be called a superconducting antiferromagnet or an antiferromagnetic superconductor. d-wave superconductivity exists by itself at large electron or hole doping. The transition from a homogeneous coexistence phase to pure d-wave superconductivity is second order, except for large values of $U = 12t$ on the electron-doped side. Qualitatively, it seems that $U = 8t$ gives a better agreement with the experimental phase diagram of the cuprates since, in that case, superconductivity appears alone over a broader range of dopings on the hole than on the electron-doped side. Also, the value of the maximum d-wave order parameter is larger on the hole- than on the electron-doped side, showing that competition with antiferromagnetism can reverse the trend observed as a function of t' in Fig. 2. Choosing a value of U on the electron-doped side[43,44] that is smaller than the value of U for the hole-doped side would also help in making the tendency for d-wave superconductivity smaller on the electron-doped side, as observed experimentally. The asymmetry in the maximum value of the d-wave order parameter for hole and electron doping is also observed for $U = 6t$, but in that case the antiferromagnetism occurs over a doping range that is unreasonably large compared to the experiment. For $U = 8t$, optimal doping occurs around 15% in the hole-doped case. $U = 8t$ is also consistent with the value necessary to explain details of the spin wave spectrum obtained by neutron measurements at half-filling.[45,46] All these qualitative trends agree with the experimental phase diagram except for the following: antiferromagnetism extends over a broader range of dopings on the hole-doped side than experimentally observed (see, however, the next section) and there is a strong tendency for homogeneous coexistence of the two order parameters, even though the d-wave order parameter is suppressed by the presence of antiferromagnetic order. While the suppression of d-wave superconductivity by antiferromagnetism is appreciable, the reverse effect is almost negligible.[47] This is also observed in mean-field studies.[48]

Homogeneous coexistence of antiferromagnetism and d-wave superconductivity is not generic in the cuprates. Nevertheless, it has been observed recently in ordered layered compounds[49] and in the electron-doped cuprate PrCeCuO.[50] Although such coexistence is not observed in compounds such as $YBa_2Cu_3O_{7-x}$ (YBCO), it appears in $La_2CuO_{4.11}$ at zero field and in $La_{1.9}Sr_{0.1}CuO_4$ under applied magnetic field.[51] The agreement of the latter field-dependent experiments[52] with the theoretical predictions[53] reveals the proximity of single-phase d-wave superconductivity with homogeneous coexistence of antiferromagnetism and d-wave superconductivity. Other $La_{2-x}Sr_xCuO_4$ (LSCO) compounds[54,55] reveal the proximity of antiferromagnetism and d-wave superconductivity through the application of a magnetic field. Muon spin rotation studies as a function of

doping, temperature, and field show that the zero-field coexistence of superconductivity with short-range static magnetism[56] is generic in the underdoped regime. Since competition between antiferromagnetism and d-wave superconductivity seems to be quite sensitive to disorder,[57] the homogeneous coexistence between the two phases that we find here may be reconcilable with experiments.

It is instructive to compare our theoretical results with other approaches that include competition of d-wave superconductivity with antiferromagnetism. Early variational calculations[58] at $t'=0$, $U=10$, and with the $t-J$ model[59] showed a strong tendency for antiferromagnetism and superconductivity to coexist homogeneously, even though there is a region where d-wave superconductivity exists by itself. The most recent variational calculations[40,60] show the same trend. Weak-coupling calculations with functional renormalization coupled to renormalized mean-field theory at $U=2.5$ and $t'=-0.15$ also show a coexistence region.[28] A recent review[33] of variational approaches and renormalized mean-field theory results[61] shows that a coexistence region is often obtained in these approaches, as it was in early slave-boson theories.[36]

An early version of cluster DMFT[62] using $t'=-0.15t$ and $U=4.8t$ found that d-wave superconductivity and antiferromagnetism coexist over most of the doping range $1-n$ <0.3. Recent CDMFT calculations[63] at $t'=0$ find that an homogeneous coexistence region appears at weak coupling but is replaced by a first-order transition between both phases at strong coupling. Phase separation as a function of doping takes place in strong coupling but not in weak coupling. Here, at finite t', we did find a first-order transition at large U on the electron-doped side but phase coexistence persists at low doping.

In VCA calculations that include cluster chemical potential as a variational parameter[64,65] to ensure thermodynamic consistency, a coexistence phase with continuous transition to d-wave superconductivity is found for $t'=-0.3$ at weak coupling, but at strong coupling the transition between homogeneous coexistence and pure d-wave superconductivity is first order,[66] as we have found here for $U=12t$ on the electron-doped side. In early VCA studies,[67] $U=8$, $t'=-0.3$, it was noticed that the energy scale for that first-order transition is larger on the hole than on the electron-doped side. In VCA calculations that do not include chemical potential as a variational parameter, zero-temperature finite-size studies find antiferromagnetism and d-wave superconductivity over doping ranges that agree semi-quantitatively with experiment for both hole- and electron-doped systems,[30] using $U=8t$ and taking the second nearest neighbor hopping parameter $t'=-0.3t$ and the third nearest neighbor hopping $t''=0.2t$ from the band structure. As in our case, there is a coexistence region on the electron-doped side, but on the hole-doped side there is still some nonmonotonic size dependence that suggests that inhomogeneous phases may be more stable.

Finally, in DCA, system sizes up to 32 sites have been studied for $U=4t$, $t'=0$. At 10% doping, a superconducting transition is found[68] with critical temperature $T_c=0.023$. The question of ground state coexistence was not studied since these are finite temperature studies. However, it was established at intermediate coupling that the frequency and momentum dependence of the pairing channel comes from the antiferromagnetic fluctuations.[69–71] Within DCA, there is a tendency for phase separation in the normal state on the electron-doped side of the phase diagram.[72] The same tendency is observed at weak coupling[73] using the two-particle self-consistent (TPSC) approach.[74]

D. Additional effects of the band structure on the phase diagram

The one-band Hubbard model is an effective model of the cuprates, so parameters can vary with doping.[43,44] Given our numerical uncertainties, it would be inappropriate at this point to fine tune our parameters to try to find a best fit of the experimental phase diagram of the high-temperature superconductors. Nevertheless, we point out in this section that when more realistic band parameters are used for the calculation, the qualitative changes of the resulting phase diagram go in the right direction to improve agreement with experiment. We also comment on the implications of sensitivity to band parameters.

The most common parameters used for the one-band model of YBCO, for example,[42,75] are $t'=-0.3t$, $t''=0.2t$, where t'' stands for the third nearest neighbor hopping. It has been known for a decade[76] that for the half-filled parent compound $Sr_2CuO_2Cl_2$, for example, these values well describe ARPES experiments. Adding the third nearest neighbor hopping $t''=0.2t$ to the calculation of the previous section leads to the phase diagram illustrated on the upper part of Fig. 4. Clearly, the phase diagram becomes qualitatively closer to that of the cuprates since the antiferromagnetic phase has a stronger electron-hole asymmetry and the tendency for coexistence between antiferromagnetism and d-wave superconductivity is reduced. These two results were found first in recent VCA calculations.[77] Note also that the phase boundaries for antiferromagnetism are extremely close to those obtained from VCA for the same parameters.[30] In our CDMFT calculations, the effect of t'' enters only in the self-consistency condition [Eq. (4)] through the parameter $\hat{t}(\widetilde{\mathbf{k}})$ of the superlattice Green function [Eq. (5)]. In VCA, the clusters are larger so that t'' can also enter in the cluster calculation not only in the self-consistency condition. The excellent agreement between both methods for the boundaries of the antiferromagnetic phases suggests that the main effect of t'' is taken into account in our CDMFT calculations.

In the lower part of Fig. 4, one finds the phase diagram corresponding to parameters typical of LSCO,[42] namely, t' $=-0.17t$ and $t''=0.08t$. There are quantitative changes compared to the top figure appropriate for YBCO. In particular, on the hole-doped side of the phase diagram, the d-wave phase extends to larger dopings for the above LSCO parameters than those for YBCO. Although there is no qualitative change, this quantitative sensitivity of the phase diagram to band parameters suggests that the universality of the $T_c(\delta)/T_c^{max}$ relation,[78,79] which is usually assumed for hole-doped (δ) high-temperature superconductors, may not be completely accurate, unless it signals that band parameters are, in fact, quite close, as has been suggested in some recent studies.[46] The possible lack of universality of the $T_c(\delta)/T_c^{max}$

FIG. 5. The gap as a function of filling, for $U=8t$, $t'=-0.3t$. The gap is defined as half the distance between the two peaks on either side of $\omega=0$, as they appear, for example, in the inset.
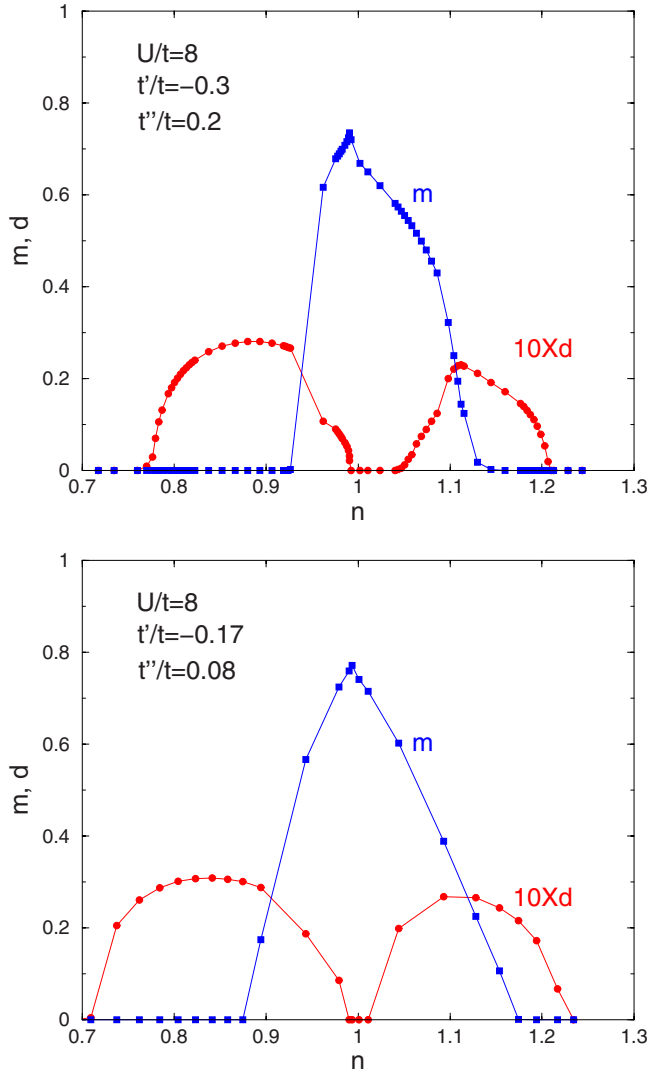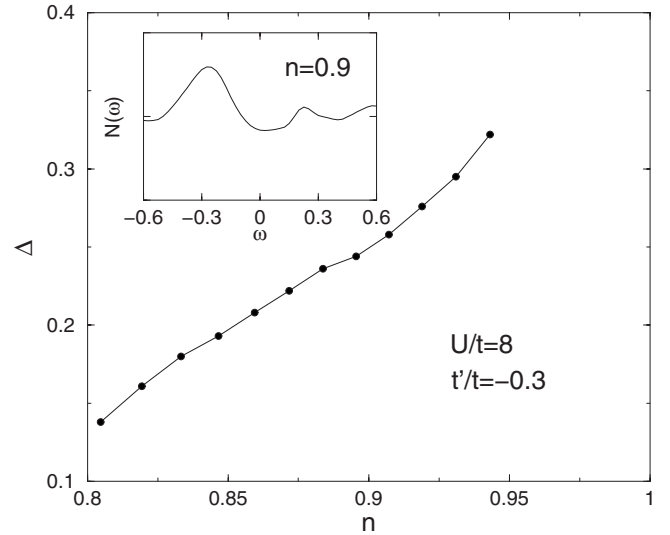
FIG. 4. (Color online) Superconducting (red circles) and antiferromagnetic (blue squares) order parameters for $U=8t$ and various values of the band parameters. On the top, parameters $t'=-0.3t$, $t''=0.2t$ appropriate for YBCO. On the bottom, $t'=-0.17t$, $t''=0.08t$ as in LSCO. The amplitude of the superconducting order parameter is multiplied by a factor of 10 to be on a comparable scale with the antiferromagnetic one.

relation has been noticed before.[75] In experiments, it has been pointed out a while ago[80] that single layer $Bi_2Sr_{2-z}La_zCu_2O_{6+\delta}$ (BSLCO) deviates from the universal $T_c(\delta)/T_c^{max}$ curve. The electronic structure of that compound differs[81] from that of LSCO, which is the compound used to determine the universal $T_c(\delta)/T_c^{max}$ curve.[78] Hence, the band structure could be one of the factors explaining the deviations of single layer BSLCO. There is also a "universal" $T_c[S(290 \text{ K})]/T_c^{max}$ determined from thermopower $S(290 \text{ K})$ at 290 K instead of doping.[79] However, thermopower has been experimentally linked to the band structure.[82]

E. Gap in total density of states and angle-resolved photoemission spectroscopy spectrum

Having established that the d-wave order parameter ψ decreases toward zero as we approach half-filling, we now

show that the gap Δ computed from the single-particle density of states increases monotonically toward half-filling $n=1$ in the hole-doped case. All the calculations of this section are for $t'=-0.3t$ and $U=8t$. The local density of states can be obtained from the cluster or from the lattice Green function. The results are identical in the limit of infinite bath size. The single-particle gap is extracted from the local density of states that we obtain from the lattice Green function that will be used later to obtain the single-particle spectral weight $A(\mathbf{k},\omega=0)$. The lattice Green function is computed by periodizing the superlattice Green function $G^{\mu\nu}(\widetilde{\mathbf{k}},\omega)$ in Eq. (5) over the entire Brillouin zone of the original infinite lattice as is done in CPT.[43] This proceeds as follows. In reciprocal space, any wave vector $\mathbf{k}$ in the Brillouin zone may be written as $\mathbf{k}=\widetilde{\mathbf{k}}+\mathbf{K}$, where both $\mathbf{k}$ and $\widetilde{\mathbf{k}}$ are continuous in the infinite-size limit. However, $\widetilde{\mathbf{k}}$ is only defined in the reduced Brillouin zone that corresponds to the superlattice. On the other hand, $\mathbf{K}$ is discrete and denotes reciprocal lattice vectors of the superlattice. Then, the lattice Green function is defined by

$$G_{\text{latt}}(\mathbf{k},\omega) = \sum_{\mu,\nu} e^{-i\mathbf{k}\cdot(r_\mu-r_\nu)} G^{\mu\nu}(\mathbf{k},\omega), \qquad (9)$$

where $G^{\mu\nu}(\mathbf{k},\omega)=G^{\mu\nu}(\widetilde{\mathbf{k}},\omega)$. Integration over $\mathbf{k}$ yields the local density of states. Different periodization procedures can be used.[9,10]

The single-particle gap is defined as half the distance between the peaks that surround the minimum near $\omega=0$. The inset of Fig. 5 shows the local density of states in the superconducting state at $n=0.9$. Due to the finite value of the broadening parameter $(0.1t)$, some spectral weight fills the d-wave gap, which linearly vanishes near $\omega=0$. We do not focus on this $\omega \rightarrow 0$ energy scale. In Fig. 5, we exhibit the monotonic increase of the single-particle gap as filling increases toward $n=1$ (unlike the order parameter decrease) in
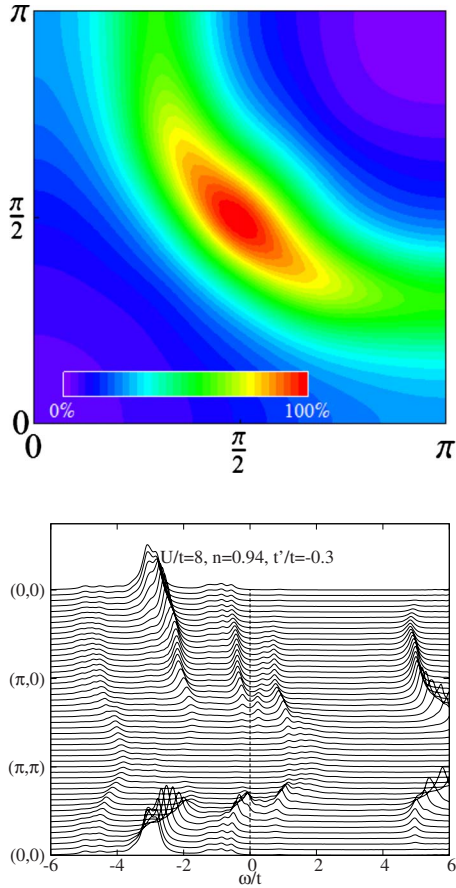
FIG. 6. (Color online) Hole-doped *d*-wave superconducting phase for $n=0.94$, $U=8t$, $t'=-0.3$. Upper figure, color contour plot of $A(\mathbf{k},\omega=0^+)$ in the first quadrant of the Brillouin zone. Energy resolution is $\eta=0.1t$ for both figures. Lower figure, $A(\mathbf{k},\omega)$ for various values of wave vector along high-symmetry directions. The relative scale in the contour plot can be made quantitative by comparison with the lower figure.
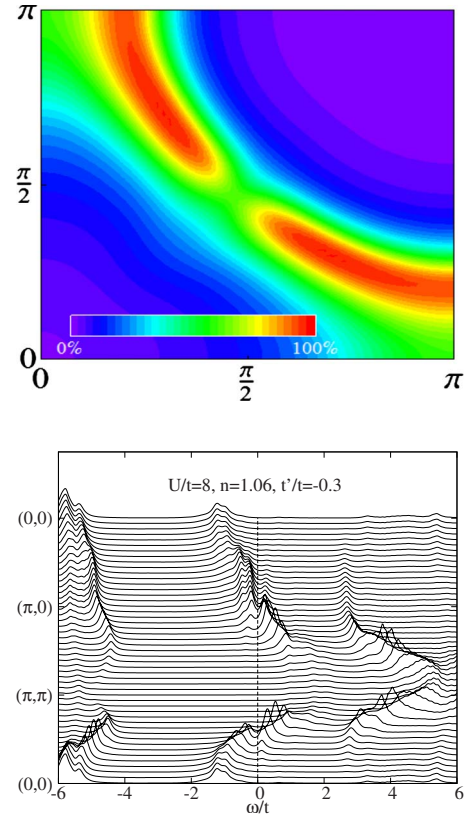

FIG. 7. (Color online) Same plots as in Fig. 6 but for the electron-doped case $n=1.06$. The maximum on the color scale corresponds to 104% of the maximum of the data to stress finer details near the maximum. All other parameters are identical.

accordance to, for example, thermal conductivity[1] and tunneling experiments[83,84] for the cuprates. This is a radical departure from a conventional superconductor where the single-particle gap Δ and ψ are proportional to each other. Experimentally in the hole-doped cuprates,[1] the magnitude of the gap at optimal doping is estimated to be around 50 meV. Here, we obtain $0.2t$, which is in good agreement with experimental estimates if we take a reasonable value $t=250$ meV. CDMFT should be reliable for the value of this gap since it is extracted from a local quantity.

In Figs. 6 and 7, we present single-particle spectra in the *d*-wave superconducting state for, respectively, hole doping $n=0.94$ and electron doping $n=1.06$. The upper part of the figures illustrates the momentum distribution curves (MDCs) at the Fermi energy in the first quadrant of the Brillouin zone, in other words, a contour plot of the single-particle spectral weight $A(\mathbf{k},\omega=0)$ with a finite energy resolution $\eta=0.1t$. The lower part contains energy distribution curves (EDCs) $A(\mathbf{k},\omega)$ as a function of frequency in units of *t* for various wave vectors $\mathbf{k}$ along symmetry directions.

The MDC for hole doping, $n=0.94$, in Fig. 6, and electron doping, $n=1.06$, in Fig. 7, are very similar to the corresponding results in the normal state obtained earlier with the same approach (Figs. 5 and 6 of Ref. 21 and Fig. 4 of Ref. 20) and with CPT,[43,85] the latter having the best momentum resolution. They display the striking asymmetry of the hole- and electron-doped cases that can be measured by ARPES in the *d*-wave superconducting phase[22] and in the pseudogap phase. More specifically, for the hole-doped case, the Fermi energy plot (MDC) shows weight near $(\pi/2,\pi/2)$ with a clear suppression everywhere else. On the other hand, the electron-doped case (Fig. 7) shows weight in complementary areas of $(\pi,0)$ and $(0,\pi)$ with the largest suppression near $(\pi/2,\pi/2)$.

As shown in an earlier paper,[21] it is likely that for large values of *U*, the correlations responsible for the suppressed weight in the normal state are of short-range antiferromagnetic origin, although the precise nature of the magnetic fluctuations seems less important than the fact that the system is close to a Mott insulator[20] and that there are short-range spatial magnetic correlations induced by *J*. This is the strong-coupling mechanism for pseudogap discussed in Refs. 43 and 85. By contrast, the weak-coupling mechanism does not need to be close to a Mott insulator. It involves long wavelength fluctuations[44,74,86] that can be explained by the two-particle self-consistent approach. The latter mechanism seems to explain[86] experimental results in slightly underdoped $Nd_{2-x}Ce_xCuO_4$. For a discussion of the pseudogap at large and small *U*, see Refs. 43 and 85.

In the EDC for the hole-doped case on the lower part of Fig. 6, one can see in the $(0,0)$ to (π,π) direction a gaplike feature between $-t$ and $-2t$ that looks like the so-called waterfall feature observed in ARPES experiments.[87–92] This has some similarity to what has been obtained in the t-J model[93] but one should be careful since at these energy scales, it is likely that the one-band Hubbard model differs from more realistic multiband models.[3] The gaplike feature here occurs between the spin-fluctuation-induced band near the Fermi energy[21] and the rest of the lower-Hubbard band. There are differences with DMFT calculations since these are appropriate only for higher dimension.[94]

In the hole-doped case of Fig. 6, we do not have the resolution to address the question of whether there are two gaps, one associated with superconductivity and the other one associated with the pseudogap, as discussed recently in the literature.[95–98] This question is clearly most difficult to address in the hole-doped compounds where the pseudogap and superconducting gap occur in the same region of the Brillouin zone. In the electron-doped case of Fig. 7, the position of the pseudogap or of the antiferromagnetic gap near $(\pi/2,\pi/2)$ differs from the location of the maximum superconducting gap. Hence, an earlier VCA study[30] with better momentum resolution allowed one to see the superconducting gap in the electron-doped case near $(\pi,0)$ at the same time as the (pseudo)gap near $(\pi/2,\pi/2)$. In our case also, the EDC in the lower part of Fig. 7 does have both the normal state gap near $(\pi/2,\pi/2)$ and the d-wave superconducting gap near $(\pi,0)$. The MDC color scheme in the upper part of the same figure is on a relative scale. Hence, despite the fact that there is both a pseudogap and a superconducting gap, the MDC emphasizes that there is less weight in the pseudogap region near $(\pi/2,\pi/2)$ than near the superconducting gap region near $(\pi,0)$, $(0,\pi)$. Nevertheless, close inspection reveals that regions of constant intensity carry less weight near $(\pi,0)$ than the corresponding normal state results in Ref. 21. Also, the weight increases as one moves slightly away from the zone edge along the Fermi surface, reflecting the superconducting gap. Experimentally, the superconducting gap in the electron-doped compounds has been seen independent of the pseudogap.[99]

IV. CONCLUSION

A. Summary

We have shown that many of the non-BCS features exhibited by superconductivity in the underdoped cuprates can be reproduced by CDMFT calculations for the two-dimensional Hubbard model. For example, the fact that the zero-temperature d-wave superconducting order parameter decreases as we move toward half-filling while the gap in the single-particle density of states increases, we have demonstrated semiquantitative agreement with other cluster methods and with experimental results for other quantities as well, such as the ARPES spectrum and the doping range where superconductivity is stable.

We have also calculated the phase diagram that describes the competition between antiferromagnetism and superconductivity for $t'=-0.3t$ for both hole and electron doping at various values of U. There is, in general, homogeneous coexistence (superconducting antiferromagnetism or, equivalently, antiferromagnetic superconductivity) between antiferromagnetism and d-wave superconductivity in the underdoped region. This feature is quite generally observed in quantum cluster methods, variational approaches, and mean-field theories that do not allow for spin or charge density modulations on large length scales. In experiment, such coexistence seems to be the exception rather than the norm. At large U, the transition between the coexistence phase and the pure d-wave state is first order.

Without attempting any precise fits to experimental data, it seems that the phase diagram obtained for $t'=-0.3t$ at intermediate coupling $U=8t$ corresponds to the experimental phase diagram better than either smaller ($U=6t$) or larger ($U=12t$) values of U. Interestingly, adding the third neighbor hopping $t''=0.2t$, as suggested by the band structure, leads to an improvement of the qualitative agreement between the calculated and observed phase diagrams, namely, a reduced tendency to coexistence and a larger electron-hole asymmetry. The sensitivity to band parameters, expected at intermediate coupling where both kinetic and potential contributions are comparable, hints toward quantitative deviations from the universal $T_c(\delta)/T_c^{max}$ curve for compounds with different band parameters, such as LSCO and YBCO.

B. Discussion

The major questions left open by the present work are as follows: (a) whether the Hubbard model by itself, without additional interactions, additional bands, or without extrinsic disorder, can lead to a closer agreement with the experimental phase diagram when additional broken symmetries are allowed in the space of solutions[100–103] and (b) if the additional broken symmetries that are present in cuprates appear as secondary instabilities or are essential to the physics of high-temperature superconductivity.

Nevertheless, the Hubbard model seems sufficient to lead to the overall phase diagram of the high-temperature superconductors and to explain many of the observed non-BCS features, even in the absence of a final answer to the last questions raised. In BCS theory, it is useful to think about the mechanism for superconductivity, i.e., what perturbation makes the normal state unstable toward a superconducting ground state. Similarly, in the weak-coupling Hubbard model, finite temperature DCA[69–71] and TPSC[27] suggest that in this case, it makes sense to think of d-wave superconductivity as being mediated by antiferromagnetic fluctuations,[104–107] a generalization of the Kohn–Luttinger mechanism. In this weak- to intermediate-coupling case, pairing occurs when the antiferromagnetic correlation length is large.[27,108] At strong coupling though, we have shown, which is in agreement with other approaches, that the order parameter scales with the superexchange interaction J, even when we do not allow for large antiferromagnetic correlation lengths (which in the cluster treatments are mimicked by antiferromagnetic long-range order). This shows that at strong coupling, d-wave superconductivity can directly occur from the superexchange[35,36] J, without the need for an anti-

ferromagnetic "glue" or antiferromagnon exchange, as advocated by Anderson.[109] Still, at large U, the frequency dependence of the order parameter has a complicated frequency dependence with multiple scales present[110].

Antiferromagnetism and d-wave superconductivity are two possible phases of the strong-coupling Hubbard model. The normal state found in CDMFT is unstable to either phase or to a coexistence phase, depending on parameters and on doping. The CDMFT normal state contains both types of fluctuations, d wave and antiferromagnetic. At strong coupling, it does not appear necessary to think that antiferromagnetic fluctuations lead to d-wave superconductivity or that d-wave superconducting fluctuations lead to antiferromagnetism. This is perhaps best illustrated by the layered organic conductors that can be modeled by a one-band Hubbard model on the anisotropic triangular lattice at half-filling. There, one finds, theoretically and experimentally, a first-order transition between antiferromagnetism and d-wave superconductivity,[6,7] so both phases are different instabilities of the same Hamiltonian.

CDMFT and a number of methods show that maximum pairing (maximum value of the d-wave order parameter) occurs at intermediate coupling, a range appropriate for the high-temperature superconductors. So, both weak- and strong-coupling features may appear.[69–71]

One of the ways to distinguish weak- and strong-coupling limits is by the behavior of the d-wave order parameter as one approaches half-filling. At strong coupling, it decreases as $n \to 1$ when U is larger than the critical U for Mott localization. The phase fluctuations and short-range antiferromagnetic correlations that lead to the decrease need not be long range: they occur within the cluster. At weak coupling on the other hand, the decrease in the order parameter near half-filling does not occur unless antiferromagnetic fluctuations with correlation lengths large enough to create the pseudogap are included.[27,108] Exactly at half-filling, weak- and strong-coupling limits are separated in the normal state by the Mott transition,[19,111] in the absence of magnetic long-range order. Away from half-filling, one can postulate that when the correlation length of the antiferromagnetic fluctuations become of the order of the lattice spacing, then J by itself suffices to lead to pairing at strong coupling. There may not be a sharp phase transition between the two extreme limits.

Quantum cluster methods are powerful numerical ways of attacking the problem of high-temperature superconductivity. They clearly show that many aspects of the physics of the high-temperature superconductors are contained in the Hubbard model. The convergence between the results of these methods and those of other recent numerical approaches suggests that we are closing in on methods that can provide a quantitative solution of this problem.

[1] M. Sutherland *et al.*, Phys. Rev. B **67**, 174520 (2003).

[2] M. B. J. Meinders, H. Eskes, and G. A. Sawatzky, Phys. Rev. B **48**, 3916 (1993).

[3] A. Macridin, M. Jarrell, T. Maier, and G. A. Sawatzky, Phys. Rev. B **71**, 134527 (2005).

[4] B. J. Powell and R. H. McKenzie, J. Phys.: Condens. Matter **18**, R827 (2006).

[5] G. Kotliar, S. Y. Savrasov, G. Pálsson, and G. Biroli, Phys. Rev. Lett. **87**, 186401 (2001).

[6] B. Kyung and A.-M. S. Tremblay, Phys. Rev. Lett. **97**, 046402 (2006).

[7] P. Sahebsara and D. Sénéchal, Phys. Rev. Lett. **97**, 257004 (2006).

[8] T. Maier, M. Jarrell, T. Pruschke, and M. H. Hettler, Rev. Mod. Phys. **77**, 1027 (2005).

[9] A. M. S. Tremblay, B. Kyung, and D. Senechal, Low Temp. Phys. **32**, 424 (2006).

[10] G. Kotliar, S. Y. Savrasov, K. Haule, V. S. Oudovenko, O. Parcollet, and C. A. Marianetti, Rev. Mod. Phys. **78**, 865 (2006).

[11] A. Georges, G. Kotliar, W. Krauth, and M. Rozenberg, Rev. Mod. Phys. **68**, 13 (1996).

[12] M. Jarrell, Phys. Rev. Lett. **69**, 168 (1992).

[13] M. H. Hettler, A. N. Tahvildar-Zadeh, M. Jarrell, T. Pruschke, and H. R. Krishnamurthy, Phys. Rev. B **58**, R7475 (1998).

[14] M. Potthoff, M. Aichhorn, and C. Dahnken, Phys. Rev. Lett. **91**, 206402 (2003).

[15] M. Potthoff, Eur. Phys. J. B **32**, 429 (2003).

[16] G. Biroli and G. Kotliar, Phys. Rev. B **71**, 037102 (2005).

[17] C. J. Bolech, S. S. Kancharla, and G. Kotliar, Phys. Rev. B **67**, 075110 (2003).

[18] M. Capone, M. Civelli, S. S. Kancharla, C. Castellani, and G. Kotliar, Phys. Rev. B **69**, 195105 (2004).

[19] O. Parcollet, G. Biroli, and G. Kotliar, Phys. Rev. Lett. **92**, 226402 (2004).

[20] M. Civelli, M. Capone, S. S. Kancharla, O. Parcollet, and G. Kotliar, Phys. Rev. Lett. **95**, 106402 (2005).

[21] B. Kyung, S. S. Kancharla, D. Senechal, A.-M. S. Tremblay, M. Civelli, and G. Kotliar, Phys. Rev. B **73**, 165114 (2006).

[22] A. Damascelli, Z. Hussain, and Z.-X. Shen, Rev. Mod. Phys. **75**, 473 (2003).

[23] M. Caffarel and W. Krauth, Phys. Rev. Lett. **72**, 1545 (1994).

[24] D. Poilblanc and D. J. Scalapino, Phys. Rev. B **66**, 052513 (2002).

[25] M. Civelli, arXiv:0710.2802 (unpublished).

[26] B. Kyung, G. Kotliar, and A.-M. S. Tremblay, Phys. Rev. B **73**, 205106 (2006).

[27] B. Kyung, J.-S. Landry, and A. M. S. Tremblay, Phys. Rev. B **68**, 174502 (2003).

[28] J. Reiss, D. Rohe, and W. Metzner, Phys. Rev. B **75**, 075110 (2007).

[29] T. Maier, M. Jarrell, T. Pruschke, and J. Keller, Phys. Rev. Lett. **85**, 1524 (2000).

[30] D. Sénéchal, P.-L. Lavertu, M.-A. Marois, and A.-M. S. Tremblay, Phys. Rev. Lett. **94**, 156404 (2005).

[31] A. Paramekanti, M. Randeria, and N. Trivedi, Phys. Rev. B **70**, 054504 (2004).

[32] S. Sorella, G. B. Martins, F. Becca, C. Gazza, L. Capriotti, A. Parola, and E. Dagotto, Phys. Rev. Lett. **88**, 117002 (2002).

[33] B. Edegger, V. Muthukumar, and C. Gros, Adv. Phys. **56**, 927 (2007).

[34] P. Lee, arXiv:0708.2115 (unpublished).

[35] G. Kotliar and J. Liu, Phys. Rev. Lett. **61**, 1784 (1988).

[36] M. Inui, S. Doniach, P. J. Hirschfeld, and A. E. Ruckenstein, Phys. Rev. B **37**, R2320 (1988).

[37] M. Capone, M. Fabrizio, C. Castellani, and E. Tosatti, Science **296**, 2364 (2002).

[38] M. Capone, M. Fabrizio, C. Castellani, and E. Tosatti, Phys. Rev. Lett. **93**, 047001 (2004).

[39] R. Ofer, G. Bazalitsky, A. Kanigel, A. Keren, A. Auerbach, J. S. Lord, and A. Amato, Phys. Rev. B **74**, 220508(R) (2006).

[40] L. Spanu, M. Lugas, F. Becca, and S. Sorella, Phys. Rev. B **77**, 024510 (2008).

[41] S. R. White and D. J. Scalapino, Phys. Rev. B **60**, R753 (1999).

[42] E. Pavarini, I. Dasgupta, T. Saha-Dasgupta, O. Jepsen, and O. K. Andersen, Phys. Rev. Lett. **87**, 047003 (2001).

[43] D. Sénéchal and A.-M. S. Tremblay, Phys. Rev. Lett. **92**, 126401 (2004).

[44] B. Kyung, V. Hankevych, A.-M. Daré, and A.-M. S. Tremblay, Phys. Rev. Lett. **93**, 147004 (2004).

[45] R. Coldea, S. M. Hayden, G. Aeppli, T. G. Perring, C. D. Frost, T. E. Mason, S.-W. Cheong, and Z. Fisk, Phys. Rev. Lett. **86**, 5377 (2001).

[46] J.-Y. P. Delannoy, M. J. P. Gingras, P. C. W. Holdsworth, and A.-M. S. Tremblay (unpublished).

[47] See Fig. 49 of Ref. 9.

[48] B. Kyung, Phys. Rev. B **62**, 9083 (2000).

[49] H. Mukuda, M. Abe, Y. Araki, Y. Kitaoka, K. Tokiwa, T. Watanabe, A. Iyo, H. Kito, and Y. Tanaka, Phys. Rev. Lett. **96**, 087001 (2006).

[50] P. Dai, H. J. Kang, H. A. Mook, M. Matsuura, J. W. Lynn, Y. Kurita, S. Komiya, and Y. Ando, Phys. Rev. B **71**, 100502(R) (2005).

[51] R. J. Birgeneau, C. Stock, J. M. Tranquada, and K. Yamada, J. Phys. Soc. Jpn. **75**, 111003 (2006).

[52] B. Khaykovich, Y. S. Lee, R. W. Erwin, S.-H. Lee, S. Wakimoto, K. J. Thomas, M. A. Kastner, and R. J. Birgeneau, Phys. Rev. B **66**, 014528 (2002).

[53] Y. Zhang, E. Demler, and S. Sachdev, Phys. Rev. B **66**, 094501 (2002).

[54] B. Lake *et al.*, Science **291**, 1759 (2001).

[55] J. Chang *et al.*, Phys. Rev. Lett. **98**, 077004 (2007).

[56] J. Sonier, Rep. Prog. Phys. **70**, 1717 (2007).

[57] E. Dagotto, Science **309**, 257 (2005).

[58] T. Giamarchi and C. Lhuillier, Phys. Rev. B **47**, 2775 (1993).

[59] A. Himeda and M. Ogata, Phys. Rev. B **60**, R9935 (1999).

[60] M. Randeria (private communication).

[61] W.-Q. Chen, K.-Y. Yang, T. M. Rice, and F. C. Zhang, arXiv:0706.3556 (unpublished).

[62] A. I. Lichtenstein and M. I. Katsnelson, Phys. Rev. B **62**, R9283 (2000).

[63] M. Capone and G. Kotliar, Phys. Rev. B **74**, 054513 (2006).

[64] M. Aichhorn, E. Arrigoni, M. Potthoff, and W. Hanke, Phys. Rev. B **74**, 024508 (2006).

[65] M. Aichhorn, E. Arrigoni, M. Potthoff, and W. Hanke, Phys. Rev. B **74**, 235117 (2006).

[66] M. Aichhorn, E. Arrigoni, M. Potthoff, and W. Hanke, Phys. Rev. B **76**, 224509 (2007).

[67] M. Aichhorn and E. Arrigoni, Europhys. Lett. **72**, 117 (2005).

[68] T. A. Maier, M. Jarrell, T. C. Schulthess, P. R. C. Kent, and J. B. White, Phys. Rev. Lett. **95**, 237001 (2005).

[69] T. A. Maier, M. Jarrell, and D. J. Scalapino, Phys. Rev. B **75**, 134519 (2007).

[70] T. A. Maier, M. Jarrell, and D. J. Scalapino, Phys. Rev. B **74**, 094513 (2006).

[71] T. A. Maier, M. S. Jarrell, and D. J. Scalapino, Phys. Rev. Lett. **96**, 047005 (2006).

[72] A. Macridin, M. Jarrell, T. Maier, P. R. C. Kent, and E. D'Azevedo, Phys. Rev. Lett. **97**, 036401 (2006).

[73] S. Roy (unpublished).

[74] Y. Vilk and A.-M. Tremblay, J. Phys. I **7**, 1309 (1997).

[75] R. S. Markiewicz, S. Sahrakorpi, M. Lindroos, H. Lin, and A. Bansil, Phys. Rev. B **72**, 054519 (2005).

[76] P. W. Leung, B. O. Wells, and R. J. Gooding, Phys. Rev. B **56**, 6320 (1997).

[77] M. Guillot, M.Sc. thesis, Université de Sherbrooke, 2007.

[78] M. Presland, J. Tallon, R. Buckley, R. Liu, and N. Flower, Physica C **176**, 95 (1991).

[79] S. D. Obertelli, J. R. Cooper, and J. L. Tallon, Phys. Rev. B **46**, 14928 (1992).

[80] Y. Ando, Y. Hanaki, S. Ono, T. Murayama, K. Segawa, N. Miyamoto, and S. Komiya, Phys. Rev. B **61**, R14956 (2000).

[81] T. Kondo, T. Takeuchi, U. Mizutani, T. Yokoya, S. Tsuda, and S. Shin, Phys. Rev. B **72**, 024533 (2005).

[82] Y. Okada, H. Ikuta, T. Kondo, and U. Mizutani, Physica C **426**, 386 (2005).

[83] C. Renner, B. Revaz, J.-Y. Genoud, K. Kadowaki, and O. Fischer, Phys. Rev. Lett. **80**, 149 (1998).

[84] T. Timusk and B. Statt, Rep. Prog. Phys. **62**, 61 (1999).

[85] V. Hankevych, B. Kyung, A.-M. Daré, D. Sénéchal, and A.-M. Tremblay, J. Phys. Chem. Solids **67**, 189 (2006).

[86] E. Motoyama, G. Yu, I. Vishik, O. Vajk, P. Mang, and M. Greven, Nature (London) **445**, 186 (2007).

[87] B. P. Xie *et al.*, Phys. Rev. Lett. **98**, 147001 (2007).

[88] J. Graf *et al.*, Phys. Rev. Lett. **98**, 067004 (2007).

[89] J. Graf, G. H. Gweon, and A. Lanzara, Physica C **460**, 194 (2007).

[90] Z.-H. Pan *et al.*, arXiv:cond-mat/0610442 (unpublished).

[91] W. Meevasana *et al.*, Phys. Rev. B **75**, 174506 (2007).

[92] T. Valla, T. E. Kidd, W.-G. Yin, G. D. Gu, P. D. Johnson, Z.-H. Pan, and A. V. Fedorov, Phys. Rev. Lett. **98**, 167003 (2007).

[93] F. Tan, Y. Wan, and Q.-H. Wang, Phys. Rev. B **76**, 054505 (2007).

[94] K. Byczuk, M. Kollar, K. Held, Y. F. Yang, I. A. Nekrasov, T. Pruschke, and D. Vollhardt, Nat. Phys. **3**, 168 (2007).

[95] M. Le Tacon, A. Sacuto, A. Georges, G. Kotliar, Y. Gallais, D. Colson, and A. Forget, Nat. Phys. **2**, 537 (2006).

[96] K. Tanaka *et al.*, Science **314**, 1910 (2006).

[97] M. Aichhorn, E. Arrigoni, Z. B. Huang, and W. Hanke, Phys. Rev. Lett. **99**, 257002 (2007).

[98] M. Civelli, M. Capone, A. Georges, K. Haule, O. Parcollet, T. Stanescu, and G. Kotliar, Phys. Rev. Lett. **100**, 046402 (2008).

[99] N. P. Armitage *et al.*, Phys. Rev. Lett. **86**, 1126 (2001).

[100] Q. Li, M. Hücker, G. D. Gu, A. M. Tsvelik, and J. M. Tranquada, Phys. Rev. Lett. **99**, 067001 (2007).

[101] E. Berg, E. Fradkin, E.-A. Kim, S. A. Kivelson, V. Oganesyan, J. M. Tranquada, and S. C. Zhang, Phys. Rev. Lett. **99**, 127003 (2007).

[102] B. Fauqué, Y. Sidis, V. Hinkov, S. Pailhès, C. T. Lin, X. Chaud, and P. Bourges, Phys. Rev. Lett. **96**, 197001 (2006).

[103] S. A. Kivelson, I. P. Bindloss, E. Fradkin, V. Oganesyan, J. M. Tranquada, A. Kapitulnik, and C. Howald, Rev. Mod. Phys. **75**, 1201 (2003).

[104] M. T. Beal-Monod, C. Bourbonnais, and V. J. Emery, Phys. Rev. B **34**, 7716 (1986).

[105] K. Miyake, S. Schmitt-Rink, and C. M. Varma, Phys. Rev. B **34**, 6554 (1986).

[106] D. J. Scalapino, E. Loh, and J. E. Hirsch, Phys. Rev. B **34**, 8190 (1986).

[107] J. Carbotte, E. Schachinger, and D. Basov, Nature (London) **401**, 354 (1999).

[108] S. R. Hassan, B. Davoudi, B. Kyung, and A.-M. S. Tremblay, Phys. Rev. B **77**, 094501 (2008).

[109] P. W. Anderson, Science **316**, 1705 (2007).

[110] K. Haule and G. Kotliar, Phys. Rev. B **76**, 104509 (2007).

[111] A. H. Nevidomskyy, C. Scheiber, D. Sénéchal, and A.-M. S. Tremblay, Phys. Rev. B **77**, 064427 (2008).